One-Dimensional Anderson Localization in Certain Correlated Random Potentials

Pierre Lugan, Alain Aspect, Laurent Sanchez-Palencia, Dominique Delande, Benoît Grémaud, Cord A. Müller, Christian Miniatura

One-Dimensional Anderson Localization in Certain Correlated Random Potentials

P. Lugan, A. Aspect, and L. Sanchez-Palencia
Laboratoire Charles Fabry de l'Institut d'Optique, CNRS and Univ. Paris-Sud, Campus Polytechnique, RD 128, F-91127 Palaiseau cedex, France

D. Delande[1], B. Grémaud[1,2,3], C.A. Müller[1,4], and C. Miniatura[2,3,5]
[1] *Laboratoire Kastler-Brossel, UPMC, ENS, CNRS; 4 Place Jussieu, F-75005 Paris, France*
[2] *IPAL, CNRS; 1 Fusionopolis Way, Singapore 138632, Singapore*
[3] *Centre for Quantum Technologies, National University of Singapore, 3 Science Drive 2, Singapore 117543, Singapore*
[4] *Physikalisches Institut, Universität Bayreuth, D-95440 Bayreuth, Germany*
[5] *Institut Non Linéaire de Nice, UNS, CNRS; 1361 route des Lucioles, F-06560 Valbonne*
(Dated: January 31, 2009)

We investigate Anderson localization in weak 1D speckle potentials. We show that long-range correlations induce effective mobility edges corresponding to sharp crossovers between regions where localization lengths differ by orders of magnitude. Using perturbation theory, we derive analytical formulas up to two orders beyond Born approximation which prove in excellent agreement with exact numerical calculations. Finally, we analyze our findings in the light of a diagrammatic approach.

PACS numbers: 03.75.-b,42.25.Dd,72.15.Rn

Multiple scattering from random impurities strongly affects wave diffusion in imperfect media [1]. For instance, destructive interference of multiple scattering waves is responsible for Anderson localization (AL), i.e. suppression of diffusion and exponentially decaying waves [2, 3]. So far, AL has been reported for classical, light waves [4, 5], sound waves [6], microwaves [7] and in photonic crystals [8, 9], and very recently for quantum matter-waves in ultracold atomic gases [10, 11, 12]. In the latter case, controlled random potentials can be designed almost at will [13, 14], offering unprecedented possibilities to explore the role of finite-range correlations.

One-dimensional (1D) systems are peculiar as regards AL compared to higher dimensions. In 3D, there is a metal-insulator transition (*mobility edge*) given approximately by the Ioffe-Regel criterion, $kl^* \sim 1$ [15], i.e. only the states with a wavenumber k smaller than the inverse transport mean-free path l^* are localized. In 2D, all states are localized but the localization length $L_{\rm loc}$ diverges exponentially with kl^* for $kl^* > 1$. In contrast, there is no localization threshold in 1D systems and $L_{\rm loc}$ is predicted to equal l^*. However, interestingly, long-range correlations can induce anomalous diffusion effects and result in non-standard localization properties [16].

A particularly important example is that of speckles [17] as used in experiments with ultracold atoms [10]. Indeed, the power spectrum of a speckle potential has a finite support such that the Fourier transform of the disorder, $\hat{V}(q)$, vanishes for q exceeding a certain threshold $k_{\rm c}/2$. Then, the Born approximation –which is expected to be relevant for weak disorder [18]– predicts that the random potential does not provide back-scattering and thus no localization for $k > k_{\rm c}$. This property defines an *effective mobility edge* in 1D [19] at $k = k_{\rm c}$ [20], evidences of which have been reported recently [10]. In this context, questions have raised about the true nature of the *effective mobility edge* and localization properties beyond it. In particular, the question whether $k = k_{\rm c}$ defines an exact or approximate mobility edge for 1D speckle potentials have been very debated.

In this Letter, we address these questions for speckle potentials using perturbation theory beyond the Born approximation and exact numerical calculations [21]. Although related questions have been addressed earlier in different contexts [22], it is important to stress that speckle potentials have non-standard properties that make them an original class of disorder to study on their own: (i) They are non-Gaussian disorders [23] and (ii) their probability distribution is not symmetric. We find that AL occurs even beyond the effective mobility edge at $k = k_{\rm c}$. In fact, there exist several effective mobility

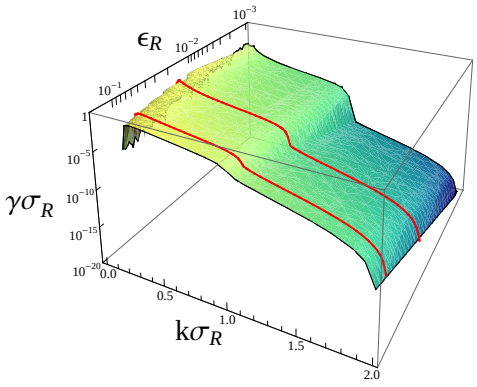

Figure 1: (color online) Lyapunov exponent γ calculated two orders beyond Born approximation versus the particle momentum k and the parameter $\epsilon_{\rm R}$ for particles in 1D speckle potentials created with a square diffusive plate. The red lines correspond to $\epsilon_{\rm R} = 0.1$ and $\epsilon_{\rm R} = 0.02$ respectively (same curves as in Fig. 3).

edges located at $k_c^{(p)} = pk_c$ with p an integer such that AL in the successive regions $k_c^{(p-1)} < k < k_c^{(p)}$ is dominated by higher and higher order scattering events. *Effective mobility edges* are thus characterized by crossovers which are sharper for weaker disorder (see Fig. 1). We prove this property for the first two effective mobility edges by calculating explicitely the three lowest orders in the Born expansion. Our analytic calculations prove in excellent agreement with numerics. Finally, we analyze our findings using diagrammatic methods.

Phase formalism – Consider a particle of energy E in a 1D random potential $V(z)$ of statistical average zero ($\langle V\rangle = 0$). Using a phase-density-like representation [18]:

$$\phi(z) = r(z)\sin\left[\theta(z)\right]; \qquad \partial_z\phi = kr(z)\cos\left[\theta(z)\right], \quad (1)$$

with $k = \sqrt{2mE/\hbar^2}$ the particle wavenumber in the absence of disorder, the Schrödinger equation in 1D is equivalent to the coupled equations

$$\partial_z\theta(z) = k\left[1 - (V(z)/E)\sin^2\left(\theta(z)\right)\right] \quad (2)$$

$$\ln[r(z)/r(0)] = k\int_0^z \mathrm{d}z'\left(V(z')/2E\right)\sin\left(2\theta(z')\right). \quad (3)$$

The phase formalism allows for a simple perturbation approach [18]: We solve Eq. (2) perturbatively in increasing powers of V and we reintroduce the solutions at different orders into Eq. (3) so as to calculate the corresponding perturbation orders of the Lyapunov exponent:

$$\gamma(k) = \lim_{|z|\to\infty}\langle \ln(r(z))/|z|\rangle = \sum_{n\geq 2}\gamma^{(n)}(k). \quad (4)$$

This approach allows one to compute the Lyapunov exponent up to any order n in the perturbation series from the n-point correlator $C_n(z_1,...,z_{n-1}) = \langle V(0)V(z_1)...V(z_{n-1})\rangle$ of the random potential. Using amplitude V_R and correlation length σ_R of the disorder as energy and length scales, the n-point correlator reads

$$C_n(z_1,...,z_{n-1}) = V_R^n c_n\left(z_1/\sigma_R,...,z_{n-1}/\sigma_R\right) \quad (5)$$

where c_n is the reduced correlation function which depends only on the model of disorder.

Applying perturbation theory up to the second order beyond Born approximation ($n = 4$), we then find

$$\gamma^{(n)} = \sigma_R^{-1}\left(\frac{\epsilon_R}{k\sigma_R}\right)^n f_n(k\sigma_R) \quad (6)$$

where $\epsilon_R = 2m\sigma_R^2 V_R/\hbar^2$ and

$$f_2(\kappa) = +\frac{1}{4}\int_{-\infty}^{0}\mathrm{d}u\; c_2(u)\cos(2\kappa u) \quad (7)$$

$$f_3(\kappa) = -\frac{1}{4}\int_{-\infty}^{0}\mathrm{d}u\int_{-\infty}^{u}\mathrm{d}v\; c_3(u,v)\sin(2\kappa v) \quad (8)$$

$$f_4(\kappa) = -\frac{1}{8}\int_{-\infty}^{0}\mathrm{d}u\int_{-\infty}^{u}\mathrm{d}v\int_{-\infty}^{v}\mathrm{d}w\; c_4(u,v,w) \times\left\{2\cos(2\kappa w)+\cos[2\kappa(v+w-u)]\right\}. \quad (9)$$

Notice that the compact form of Eq. (9) is provided oscillating terms, which may appear from contributions of c_4 that can be factorized as correlators c_2, are appropriately regularized at infinity. In Eq. (6), the coefficients $(\epsilon_R/k\sigma_R)^n$ diverge in the low-momentum limit $k \to 0$ while it is known that the exact $\gamma(k)$ remains finite for any finite ϵ_R [24]. This indicates a breakdown of the perturbative Born expansion, which is shown to be valid when $\gamma(k) \ll k$, that is when the localization length is much larger than the particle wavelength, a physically satisfactory criterion.

For zero-range correlations, i.e. for $c_2(u) \propto \delta(u)$, the Born term, $\gamma^{(2)}(k)$, does not vanish and is thus the leading order for any $k \gg \gamma^{(2)}(k)$. The situation happens to be richer in random potentials with long-range correlations. We now focus on the case of speckle potentials.

Speckle potentials – Speckle potentials originate from the interference pattern of a laser beam diffracted by a rough plate [13]. It follows from the diffraction process that the light field is an uncorrelated, complex Gaussian random variable [17]. In practice, the random potential is proportional to the intensity of the speckle field but defining the zero of energies so that $\langle V\rangle = 0$, it reads

$$V(z) = V_R\left(|a(z/\sigma_R)|^2 - \langle|a(z/\sigma_R)|^2\rangle\right). \quad (10)$$

Depending on the detuning of the laser with respect to the atomic resonance, the sign of V_R can be either positive ('blue detuning') or negative ('red detuning'). The quantities $a(u)$ are complex Gaussian variables, proportional to the light fields. Notice that all correlators, c_n, of the random potential are completely determined by the sole field-field correlator $c_a(u) = \langle a(0)^* a(u)\rangle$ through the statistical Gaussian theorem,

$$\langle a_1^*...a_p^* \times a_{p+1}...a_{p+p}\rangle = \sum_{\Pi}\langle a_1^* a_{p+\Pi(1)}\rangle...\langle a_p^* a_{p+\Pi(p)}\rangle, \quad (11)$$

where $a_{p'} = a(z_{p'}/\sigma_R)$ and Π describes all $p!$ permutations of $[1...p]$. For instance, $C_2(u) = |c_a(u)|^2$ and defining $a(u)$ so that $\langle|a(u)|^2\rangle = 1$, we have $\sqrt{\langle V(z)^2\rangle} = |V_R|$. A key property of speckles is that the Fourier transform of the field-field correlation function c_a has always a finite support owing to diffraction and finite-size effects [17, 19]:

$$\hat{c}_a(q) = 0 \qquad \text{for } |q| > k_c\sigma_R \equiv 1. \quad (12)$$

Here σ_R is defined so that $k_c\sigma_R = 1$.

Analytic results – We now apply perturbation theory within the phase formalism up to two orders beyond Born approximation ($n = 4$) for speckle potentials. The discussion below can be generalized to any kind of 1D random potential that fulfills the sole conditions (10)-(12) with similar conclusions (only explicit formulas for the functions $f_n(\kappa)$ would change). However, for the sake of clarity, we restrict our discussion to 1D speckle potentials

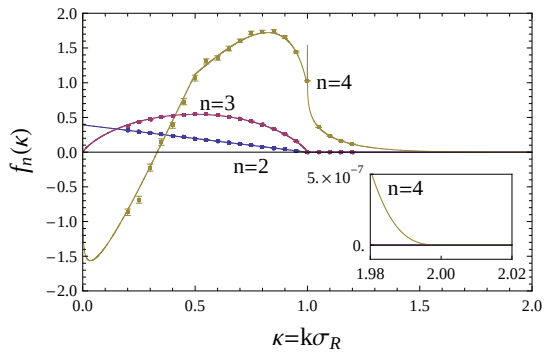

Figure 2: (color online) Functions f_n for $n = 2$, 3 and 4 for a speckle potential created with a square diffusive plate (i.e. $c_a(u) = \sin(u)/u$). The solid lines correspond to Eqs. (13)-(15) and the points with errorbars to numerical calculations. The inset is a magnification of function f_4 around $\kappa = 2$.

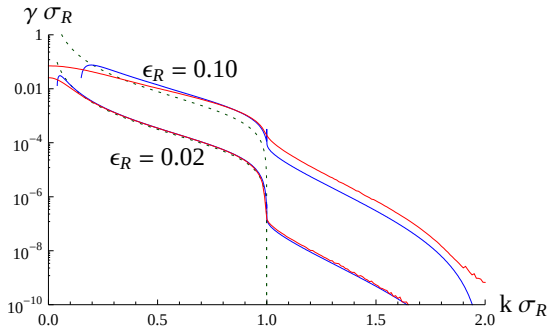

Figure 3: (color online) Lyapunov exponent $\gamma(k)$ versus the particle momentum k as determined by exact numerical calculations (red solid line) and comparison to perturbation theory up to two orders beyond Born approximation (i.e. up to $n = 4$; blue solid line). The green dashed lines are the Born term. These results hold for a speckle potential created with a square diffusive plate for two values of the parameter $\epsilon_{\rm R}$.

created by square diffusive plates as in Ref. [10] for which $c_a(u) = \sin(u)/u$. Notice that indeed, the Fourier transform of $c_a(u)$ has a finite support: $\hat{c}_a(q) \propto \Theta(1 - |q|)$ where Θ is the Heaviside step function. Inserting this correlator into Eqs. (7)-(9), we find

$$f_2(\kappa) = \frac{\pi}{8}\Theta(1-\kappa)(1-\kappa) \quad (13)$$

$$f_3(\kappa) = -\frac{\pi}{4}\Theta(1-\kappa)\left[(1-\kappa)\ln(1-\kappa) + \kappa\ln(\kappa)\right] \quad (14)$$

$$f_4(\kappa) = \frac{\pi}{64}\Big\{\Theta(1/2-\kappa)f_4^{0,\frac{1}{2}}(\kappa) + \Theta(1-\kappa)f_4^{0,1}(\kappa) + \Theta(\kappa-1)\Theta(2-\kappa)f_4^{1,2}(\kappa)\Big\}. \quad (15)$$

The functions f_2 and f_3 are simple and vanish for $\kappa > 1$ (see Fig. 2). This property is responsible for the existence of the effective mobility edge at $k = k_{\rm c}$ [19] such that $\gamma(k)\sigma_{\rm R} \sim (\epsilon_{\rm R}/k\sigma_{\rm R})^2$ for $k \lesssim \sigma_{\rm R}^{-1}$ while $\gamma(k)\sigma_{\rm R} = {\rm O}(\epsilon_{\rm R}/k\sigma_{\rm R})^4$ for $k \gtrsim \sigma_{\rm R}^{-1}$. The function $f_4(\kappa)$ has three components with three different supports: $f_4^{0,\frac{1}{2}}(\kappa)$ on $[0, 1/2]$, $f_4^{0,1}(\kappa)$ on $[0, 1]$ and $f_4^{1,2}(\kappa)$ on $[1, 2]$. The explicit formulas for $f_4^{\alpha,\beta}(\kappa)$ being quite complicated we do not reproduce them in this Letter [25]. The behavior of f_4 is actually clearer when plotted (see Fig. 2). The first cut-off is responsible for the discontinuity of the derivative of the function f_4 at $\kappa = 1/2$. At the second cut-off, $\kappa = 1$, we find a logarithmic divergence, $f_4(\kappa) \sim -2\ln|1-\kappa|$ which signals a singularity of the perturbative expansion. In addition, it is very narrow (notice that it does not appear in Fig. 1 due to the finite grid of the 3D plot) so we disregard it in the remainder of the Letter. The last cut-off at $\kappa = 2$ defines the edge of the support of the fourth-order term at $k = 2\sigma_{\rm R}^{-1}$, showing explicitly the existence of a second effective mobility edge at $k = 2\sigma_{\rm R}^{-1}$, such that $\gamma(k)\sigma_{\rm R} \sim (\epsilon_{\rm R}/k\sigma_{\rm R})^4$ for $k \lesssim 2\sigma_{\rm R}^{-1}$ while $\gamma(k)\sigma_{\rm R} = {\rm O}(\epsilon_{\rm R}/k\sigma_{\rm R})^6$ for $k \gtrsim 2\sigma_{\rm R}^{-1}$. Notice that, although the odd-n contributions do not vanish, they cannot be leading terms in any range of k. Otherwise, one would find a non-physical negative Lyapunov exponent for either $V_{\rm R} > 0$ or $V_{\rm R} < 0$.

Numerics – We have also performed exact numerical calculations using a transfer matrix approach. The results are plotted in Fig. 3 for two values of the parameter $\epsilon_{\rm R}$ relevant for the data of Ref. [10]: $\epsilon_{\rm R} = 0.02$ corresponds to $V_{\rm R}/\hbar = 2\pi \times 16$Hz in Fig. 3 of Ref. [10] and $\epsilon_{\rm R} = 0.1$ to $V_{\rm R}/\hbar = 2\pi \times 80$Hz in Fig. 3 and to Fig. 4 of Ref. [10]. For $\epsilon_{\rm R} = 0.02$, the agreement between perturbation theory and exact numerical results is excellent. In particular, the effective mobility edge at $k = \sigma_{\rm R}^{-1}$ is very clear: We find a sharp step for $\gamma(k)$ of about two orders of magnitude. The curve corresponding to $\epsilon_{\rm R} = 0.1$ shows the same trend but with a smoother and smaller step (about one order of magnitude). Although the Born approximation for $k \lesssim \sigma_{\rm R}^{-1}$ and the fourth-order term for $k \gtrsim \sigma_{\rm R}^{-1}$ provide reasonable estimates (up to a factor of about 2), higher order terms cannot be neglected. Only near $k = 0$ is the perturbative expansion unusable as expected from our discussion above.

In order to check the validity of the analytic formulas (13)-(15), we use a series of calculations of the Lyapounov exponent at fixed k and various $\epsilon_{\rm R}$ that we fit in powers of $\epsilon_{\rm R}/k\sigma_{\rm R}$. As shown in Fig. 2, the agreement with the analytic expressions is excellent. In particular, the numerics faithfully reproduce the predicted kink at $\kappa = 1/2$. The logarithmic singularity around $\kappa = 1$ is very narrow; we did not attempt to study it in detail.

Diagrammatic analysis – Diagrammatic methods provide simple graphical representations of the backscattering processes encoded in Eqs. (7)-(9) and allow to identify *effective mobility edges* quite simply. In 1D, $L_{\rm loc} = l^*$ can be calculated from the backscattering probability of $\langle|\psi|^2\rangle$ using standard quantum transport theory. The irreducible diagrams of elementary scattering events in

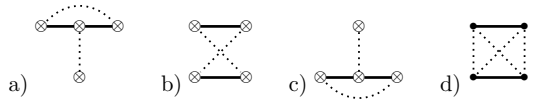

Figure 4: Relevant fourth-order backscattering contributions. Contrary to the case of uncorrelated potentials [26, 27], the sum of diagrams (a), (b) and (c) *does not* give zero for speckle potentials; only diagrams (b) and (d) contribute for $k\sigma_{\rm R} \in [1,2]$.

speckle potentials have been identified in Ref. [14].

To lowest order in $\epsilon_{\rm R}$ (Born approximation), the average intensity of a plane wave with wave vector k backscattered by the random potential is described by

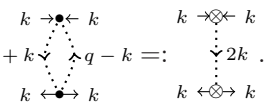

$$U_2(k) = \qquad\qquad =: \qquad . \tag{16}$$

The upper part of the diagram represents ψ (particle) and the lower part its conjugate ψ^* (hole). The dotted line $\overset{q}{\bullet\cdots\cdots\bullet} = \epsilon_{\rm R}\hat{c}_a(q)$ represents the field correlator; simple closed loops over field correlations can be written as a potential correlation $\otimes\cdots\cdots\otimes$. Backscattering requires the diagram (16) to channel a momentum $2k$, entering at the particle, down along the potential correlations to the hole. Therefore, the diagram vanishes for $k\sigma_{\rm R} > 1$.

At order $\epsilon_{\rm R}^3$, the only possible contribution is

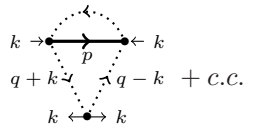

$$U_3(k) = \qquad\qquad + c.c. \tag{17}$$

The straight black line stands for the particle propagator $[E_k - E_p + i0]^{-1}$ at intermediate momentum p. The diagram (17) features two vertical field correlation lines, just as diagram (16), and thus vanishes at the same threshold $k = \sigma_{\rm R}^{-1}$. Evaluating the two-loop diagram (17), we recover precisely the contribution (14).

Many diagrams contribute to order $\epsilon_{\rm R}^4$. First there are the usual backscattering contributions with pure intensity correlations, shown in Fig. 4(a)-(c). Both 4(a) and (c) have a single vertical intensity correlation and vanish for $k > \sigma_{\rm R}^{-1}$. In contrast, the crossed diagram 4(b) has two vertical intensity correlation lines and can thus accommodate momenta up to $k = 2\sigma_{\rm R}^{-1}$. Performing the integration, we find that this diagram indeed reproduces the complicated functional dependence of those contributions to $f_4^{1,2}$ in Eq. (15) that contain factorized correlators.

Second, there are nine more diagrams, all with non-factorizable field correlations [14]. A single one has not two, but four vertical field correlation lines, shown in Fig. 4(d), and contributes for $k\sigma_{\rm R} \in [1,2]$. Carrying out the three-loop integration, we recover exactly the non-factorizable contributions to $f_4^{1,2}$ in Eq. (15).

Conclusion – In conclusion, we have shown that in speckle potentials, the k-dependence of the Lyapunov exponent exhibits sharp crossovers (*effective mobility edges*) separing regions where AL results from higher and higher scattering processes and the Lyapunov exponent changes abruptly. We have shown explicitly the existence of the first two *effective mobility edges* at $k = \sigma_{\rm R}^{-1}$ and $k = 2\sigma_{\rm R}^{-1}$. We infer that there exists a series of *effective mobility edges* at $k_{\rm c}^{(p)} = p\sigma_{\rm R}^{-1}$ with p an integer since generically, diagrams with $2p$ vertical field correlations or p intensity correlations can contribute up to $k = p\sigma_{\rm R}^{-1}$.

Stimulating discussions with P. Bouyer, V. Josse, T. Giamarchi and B. van Tiggelen are acknowledged. This research was supported by the French CNRS, ANR, MENRT, Triangle de la Physique and IFRAF.

[1] E. Akkermans and G. Montambaux, *Mesoscopic Physics of Electrons and Photons* (Cambridge Univ. Press, 2006).
[2] P. W. Anderson, Phys. Rev. **109**, 1492 (1958).
[3] P.A. Lee and T.V. Ramakrishnan, Rev. Mod. Phys. **57**, 287 (1985).
[4] D.S. Wiersma *et al.*, Nature **390**, 671 (1997).
[5] M. Störzer *et al.*, Phys. Rev. Lett. **96**, 063904 (2006).
[6] H. Hu *et al.*, Nature Phys. **4**, 945 (2008).
[7] A.A. Chabanov *et al.*, Nature **404**, 850 (2000).
[8] T. Schwartz *et al.*, Nature **446**, 52 (2007).
[9] Y. Lahini *et al.*, Phys. Rev. Lett. **100**, 013906 (2008).
[10] J. Billy *et al.*, Nature **453**, 891 (2008).
[11] G. Roati *et al.*, Nature **453**, 895 (2008).
[12] J. Chabé *et al.*, Phys. Rev. Lett. **101**, 255702 (2008).
[13] D. Clément *et al.*, New J. Phys. **8**, 165 (2006).
[14] R.C. Kuhn *et al.*, New J. Phys. **9**, 161 (2007).
[15] A.F. Ioffe and A.R. Regel, Prog. Semicond. **4**, 237 (1960).
[16] F.M. Izrailev and A.A. Krokhin, Phys. Rev. Lett. **82**, 4062 (1999).
[17] J.W. Goodman, *Speckle Phenomena in Optics: Theory and Applications* (Roberts & Company Publishers, Englewood, Colorado, 2007).
[18] I.M. Lifshits *et al.*, *Introduction to the Theory of Disordered Systems* (Wiley and sons, New York, 1988).
[19] L. Sanchez-Palencia *et al.*, Phys. Rev. Lett. **98**, 210401 (2007); New J. Phys. **10**, 045019 (2008).
[20] This effect occurs only in 1D since in 2D or 3D, any wave can be scattered by a Fourier component of the disorder with arbitrary small momentum, although possibly with a small deflection angle [14].
[21] While completing this work, we have been informed of a recent similar study; E. Gurevich, arXiv:0901.3125.
[22] L. Tessieri, J. Phys. A: Math. Gen. **35**, 9585 (2002).
[23] In laser speckles, the field $a(z)$ results from a Gaussian process. However, the random potential, $V(z) = V_{\rm R}\left(|a(z/\sigma_{\rm R})|^2 - \langle|a(z/\sigma_{\rm R})|^2\rangle\right)$, itself is not Gaussian [17].
[24] B. Derrida and E. Gardner, J. Physique **45**, 1283 (1984).
[25] Our formulas are provided as EPAPS Auxiliary Material.
[26] I.V. Gornyi *et al.*, Phys. Rev. B **75**, 085421 (2007).
[27] A. Cassam-Chenai, and B. Shapiro, J. Phys. I France **4**, 1527 (1994).

AUXILIARY MATERIAL

The functions $f_4^{\alpha,\beta}$ read

$$
\begin{aligned}
f_4^{0,\frac{1}{2}}(\kappa) &= -4\pi^2(1-2\kappa) \\
f_4^{0,1}(\kappa) &= 4-6\kappa-\frac{10\pi^2}{3}(1-2\kappa)-(4-2\kappa)\ln(\kappa) \\
&\quad -\left(\frac{5}{\kappa}-3\kappa\right)\ln(1-\kappa)+\left(\frac{1}{\kappa}+\kappa\right)\ln(1+\kappa) \\
&\quad -(4-8\kappa)\ln^2(\kappa)+22(1-\kappa)\ln^2(1-\kappa) \\
&\quad +(18+14\kappa)\ln^2(1+\kappa) \\
&\quad -16(1-\kappa)\ln(1-\kappa)\ln(\kappa) \\
&\quad -4(1-\kappa)\ln(1-\kappa)\ln(1+\kappa) \\
&\quad -32(1+\kappa)\ln(\kappa)\ln(1+\kappa) \\
&\quad -24(1+\kappa)\mathrm{Li}_2(\kappa)+32(1+\kappa)\mathrm{Li}_2\left(\frac{\kappa}{1+\kappa}\right) \\
&\quad -8\kappa\mathrm{Li}_2\left(\frac{2\kappa}{1+\kappa}\right)-8(1-2\kappa)\mathrm{Li}_2\left(2-\frac{1}{\kappa}\right) \\
f_4^{1,2}(\kappa) &= -4+2\left(1+\frac{\pi^2}{3}\right)\kappa+8\kappa\mathrm{Li}_2(1-\kappa) \\
&\quad -\left(\frac{4}{\kappa}-4+2\kappa\right)\ln(\kappa-1) \\
&\quad -4(\kappa-1)\ln^2(\kappa-1)+8\kappa\ln(\kappa-1)\ln(\kappa)
\end{aligned}
$$

where $\mathrm{Li}_2=\int_z^0 \mathrm{d}t\ \ln(1-t)/t=\sum_{k=1}^{\infty} z^k/k^2$ is the dilogarithm function.